A first principle Comparative study of electronic and optical properties of 1H – MoS2 and 2H – MoS2

ARTICLE *in* MATERIALS CHEMISTRY AND PHYSICS · AUGUST 2012

Impact Factor: 2.26 · DOI: 10.1016/j.matchemphys.2012.05.055

2 AUTHORS:

Ashok Kumar
Central University of Punjab
38 PUBLICATIONS **242** CITATIONS
SEE PROFILE

P. K. Ahluwalia
Himachal Pradesh University
123 PUBLICATIONS **468** CITATIONS
SEE PROFILE

Materials Chemistry and Physics 135 (2012) 755–761

Contents lists available at SciVerse ScienceDirect

Materials Chemistry and Physics

journal homepage: www.elsevier.com/locate/matchemphys

A first principle Comparative study of electronic and optical properties of $1H - MoS_2$ and $2H - MoS_2$

Ashok Kumar*, P.K. Ahluwalia

Physics Department, Himachal Pradesh University, Shimla 171005, Himachal Pradesh, India

HIGHLIGHTS

- Structural parameters of 2H-MoS2 and 1H-MoS2 are nearly identical.
- States around the Fermi energy are mainly due to the metal d states.
- Strong hybridization between Mo-d and S-p states below the Fermi energy has been found.
- Optical spectra of 2H-MoS2 finds very good agreements with experimental optical spectra.
- The band gap is found to be direct for 1H-MoS2 as compared to indirect for 2H-MoS2.

ARTICLE INFO

Article history:
Received 9 September 2011
Received in revised form
15 April 2012
Accepted 16 May 2012

Keywords:
Chalcogenides
Ab initio calculations
Electronic structure
Optical properties

ABSTRACT

First principle calculations of electronic and optical properties of monolayer MoS_2, so called $1H - MoS_2$, is performed which has emerged as a new direct band gap semiconductor. Before calculations of the properties of $1H - MoS_2$, we have calculated structural parameters, electronic properties (electronic band structure and electronic density of states) and frequency dependent optical response (real and imaginary part of dielectric function, energy loss function, absorption and reflectance spectra) of $2H - MoS_2$ and compared with existing experimental results and found that our calculated results are in very good agreements with experimental results. To compare the dielectric functions of bulk ($2H - MoS_2$) and monolayer ($1H - MoS_2$) phases we have further extended these calculations to the single layer MoS_2 ($1H - MoS_2$) which is analogous to graphene. Structural parameters of $1H - MoS_2$ are found very close to its bulk $2H - MoS_2$. We find direct electronic band gap at 'K' high symmetry point as compared to indirect band gap in its bulk 2H − MoS2. Our calculated dielectric function for 1H − MoS2 shows structure at nearly same energy positions as compared to 2H − MoS2 with additional structure at 3.8 eV. Also additional well defined energy loss peaks revealing the plasmonic resonances at 15.7 eV and 16.0 eV for E vector perpendicular and parallel to *c* axis respectively for 1H − MoS2 have been found, which are the signatures of surface plasmons at these energies.

1. Introduction

Two dimensional (2D) monolayers in honeycomb structure such as graphene, graphane and boron nitride have attracted growing attention due to their exotic electronic properties and exciting possibilities for applications in electronic devices [1–5]. Recently dielectric response of rippled graphene has also been subject of current investigation [6]. Although graphene is well known layered material, yet, graphene does not have a band gap, a property that is essential for many applications, in optics and transistor technology. Transition metal dichalcogenides (TMDCs) have also emerged as potential materials for many applications in optical and electronic devices because of their interesting electronic and optical properties [7–12]. Recently transition metal dichalcogenide(TMDC) semiconductor MoS_2 has attracted great interest because of its distinctive electronic, optical, catalytic and lubricating properties with exploration in diverse fields, such as nanotribology, hydrogen production, hydrodesulphurization catalyst used for removing sulphur compounds from oil, solar cells, photocatylysis [13–25]. MoS_2 is a typical example of a layered transition metal dichalcogenide family of materials. The bulk $2H - MoS_2$ crystal is built up of van der Walls bonded S–Mo–S units. Each of these stable units referred as a MoS_2 monolayer, consists of two hexagonal planes of S atoms and an intermediate hexagonal plane of Mo atoms coordinated through ionic–covalent interactions with the S atoms in

* Corresponding author. Tel.: +91 9418581622.
E-mail addresses: ashok.1777@yahoo.com (A. Kumar), pk_ahluwalia7@yahoo.com (P.K. Ahluwalia).

0254-0584/$ – see front matter © 2012 Elsevier B.V. All rights reserved.
http://dx.doi.org/10.1016/j.matchemphys.2012.05.055

a trigonal prismatic arrangement. Because of the relatively weak interactions between these layers and the strong intralayer interactions, the formation of ultrathin crystals of $1H - MoS_2$ by the micromechanical cleavage technique has been achieved by Novoselov et al. [26] who demonstrated that single 6.5 Å thick layer, with honeycomb structure can be extracted by this method. Single layer MoS_2 nanocrystal of 30 Å width have also been synthesized on Au(111) surface [27]. Liquid exfoliation of nanosheet of MoS_2 and other transition metal dichalcogenides has also been reported [28]. Very recently monolayer MoS_2 transistor has been made [29]. Other feature that makes MoS_2 interesting for nanoelectronic applications include the absence of dangling bonds and thermal stability up to 1100 °C. Various properties of $1H - MoS_2$ have been an active subject of current studies [29–36].

An extensive survey of the properties of transition metal dichalcogenides have been made by Wilson and Yoffe [7]. Beal et al. [10] measured the transmission spectra in the energy range of 0–4.0 eV and, Beal and Hughes [12] measured the reflectivity spectrum of $2H - MoS_2$ for $\vec{E} \perp c$. Hughes and Liang [11] measured the vacuum ultraviolet reflectivity spectra in the range of 4.5–14 eV for $\vec{E} \perp c$. Zeppenfeld [37] measured the electronic energy losses and optical anisotropy of single MoS_2 crystal. There are very few theoretical calculations of the optical properties in literature. Reshak and Auluck [8,9] have done full potential calculations of $2H - MoS_2$ for both $\vec{E} \perp c$ and $\vec{E} \parallel c$. But there is a lack of detailed study (experimentally and computationally) of frequency dependent optical properties of monolayer MoS_2 specified as $1H - MoS_2$. However, very recently, Johari et al. [38] have studied electron energy loss spectra (EELS) of various transition metal dichalcogenides monolayers for E vector perpendicular to c axis using plane waves based approach and Olsen et al. [39] have studied excitonic effects in monolayer MoS_2 using Bethe–Salpeter equation (BSE).

In the present paper, we have investigated the electronic and optical properties of $1H - MoS_2$ and $2H - MoS_2$ by means of ab-initio pseudopotential and numerical atomic orbitals (NAO's) basis sets based SIESTA (Spanish Initiative for Electronic Simulation with Thousand of Atoms) code and method [40–43]. We have calculated structural parameters, electronic properties and frequency dependent optical response of both $2H - MoS_2$ and $1H - MoS_2$. The results are compared with available experimental data and theoretical investigation. Both local density approximation (LDA) and generalized gradient approximation (GGA) have been used for calculation of structural and electronic parameters. Optical response has been investigated using LDA.

2. Computational details

We have used Troullier Martin, norm conserving, relativistic pseudopotential [44–47] in fully separable Kleinman and Bylander form. Local density approximation (LDA) in Ceperlay Alder (CA) parametrization as well as Perdew-Burke-Ernzerhof (PBE) variant of the generalized gradient approximation (GGA) were used for the exchange and correlation potential. All the electronic and optical calculations for both $2H - MoS_2$ and $1H - MoS_2$ are performed using calculated lattice parameters. Throughout geometry optimization, numerical atomic orbitals with double zeta polarization (DZP) basis set with a confinement energy of *30* meV were used. Relatively larger radii of the basis orbitals (using smaller value of energy shift parameter) were used for better accuracy. The convergence for energy was chosen as 10^{-5} eV between two consecutive self consistent field (SCF) steps. The total energy calculations were carried out by varying the volume of the supercell in equally spaced small steps. Minimization of energy was carried out using standard conjugate-gradients(CG) technique. Structure were relaxed until the forces on each atom were less than 0.01 *eV*/Å. Optimized (relaxed) coordinates are used for electronic structure and optical properties calculations. A $15 \times 15 \times 1$ and $30 \times 30 \times 1$ Monkhorst-Pack of k points was used for sampling Brillouin zone for calculations of structural properties and electronic structure of $1H - MoS_2$ respectively, however, $15 \times 15 \times 15$ and $30 \times 30 \times 30$ Monkhorst-Pack of k points was used for calculations of structural properties and electronic structure of $2H - MoS_2$ respectively. The spacing of the real space grid used to calculate the Hartree, exchange and correlation contribution to the total energy and Hamiltonian was *200* Ry. We have used the supercell having dimensions equal to the calculated lattice parameters (a and c) for the electronic and optical properties calculations of $2H - MoS_2$, however a 15 Å vacuum region was used for the calculations of $1H - MoS_2$ to separate the single layer along the c axis to ensure no interaction between the layers, making it effectively isolated 2D layer. Optical calculations were carried out using $90 \times 90 \times 90$ and $90 \times 90 \times 3$ optical mesh for $2H - MoS_2$ and $1H - MoS_2$ respectively. All the unoccupied states (i.e. 32 states for $1H - MoS_2$ and 64 states for $2H - MoS_2$) have been used for the calculations of optical spectra. Optical broadening of 0.2 eV has been used for optical calculations.

3. Results and discussion

3.1. Structural parameters

Molybdenum disulphide has hexagonal structure consisting of S–Mo–S layers as shown in Fig. 1. $2H - MoS_2$ has two such layers and Mo atoms of one layer are directly above the sulphur atoms of the other layer and vice-versa, while $1H - MoS_2$ has single S–Mo–S layer as shown in Fig. 1(c). We have calculated the structural parameters of $2H - MoS_2$ and $1H - MoS_2$ using both LDA and GGA as shown in Table 1. The results of $1H - MoS_2$ are compared with recently calculated values using projected augmented plane wave (PAW) based method by Ataca et al. [30,31]. We find excellent agreements with PAW based calculations as can be seen in Table 1. Also our calculated lattice parameters using GGA for $2H - MoS_2$ finds good agreements with PAW + GGA results [38] but overestimates the experimental values which is an inherent feature of standard GGA functional. Structural parameters of $2H - MoS_2$ with LDA are in very good agreement with experimentally measured values [7], although slight underestimation has been found. It is concluded that all the structural parameters calculated for $1H - MoS_2$ are nearly identical to the structural parameters calculated for $2H - MoS_2$.

3.2. Electronic band structure and density of states

The electronic band structure and corresponding total and partial density of states for $2H - MoS_2$ and $1H - MoS_2$ are shown in Fig. 2 and Fig. 3 respectively using LDA. The electronic band structure and density of states of both $2H - MoS_2$ and $1H - MoS_2$ can be divided into four group of bands and states respectively, separated by gaps. In the first group, bands in electronic band structure and states in density of states around −14 eV are mainly due to 3s orbital of S atom separated by a large gap from second group below Fermi energy in which 3 p orbital of S and 4d orbital of Mo are mainly contributing and show strong hybridization. Third group above the Fermi energy in which main contribution is due to 4d orbitals of Mo is separated by band gap from second group below Fermi energy. The fourth group above 5 eV is separated by a gap from third group has mixed Mo 5s, 4d and S 3s states. The bands on each side of the band gap are derived mainly from the 4d states of Mo in both $2H - MoS_2$ and $1H - MoS_2$. The bands around the band gap are relatively flat, as expected from the 'd' character of

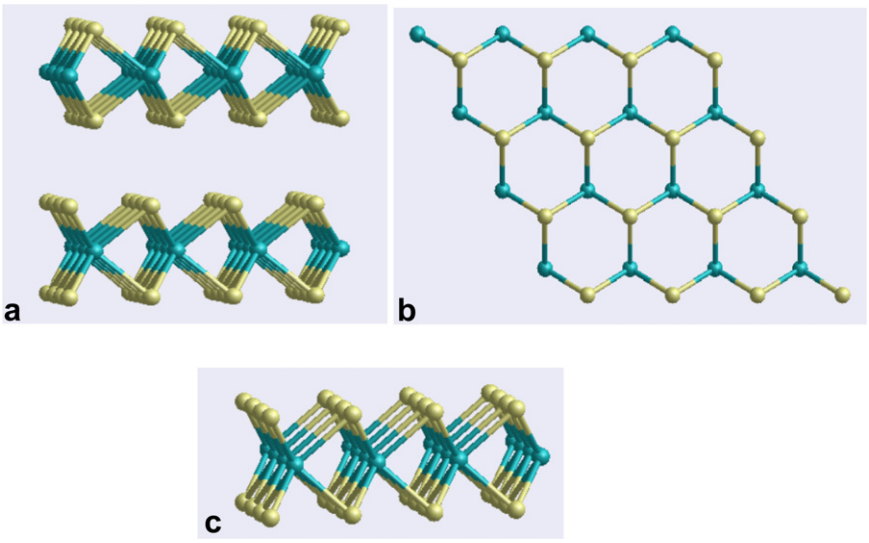

Fig. 1. (a). Side view of $2H - MoS_2$ (van der Walls bonded MoS_2 units). (b). Top view of both $2H - MoS_2$ and $1H - MoS_2$. (c). Side view of $1H - MoS_2$.

the electron states at these energies. For 2H − MoS2 the valence band maximum is at Γ and conduction band minimum is in between between Γ and K revealing indirect band semiconductor, as can be seen in Fig. 2. For 1H − MoS2 the valence band maximum and conduction band minimum is at K high symmetry point revealing direct band gap semiconductor as can be seen in Fig. 3. The details of optical interband transitions shown in Figs. 2 and 3 are discussed in next section.

The calculated and measured electronic band gap for both $2H - MoS_2$ and $1H - MoS_2$ are shown in Table 2. Although our calculated band gaps for $2H - MoS_2$ are in good agreements with other theoretical values [8,9,30,31,33], but underestimate the experimental band gap due to inherent drawback of standard LDA/GGA functionals. Our calculated value of electronic band gap for $2H - MoS_2$ using LDA + lo (GGA + lo) is 0.75 eV (1.05 eV), which is in very good agreement with 0.72 eV (0.85 eV) using LDA + PAW (GGA + PAW) based approach by Ataca et al. [30,31]. Our calculated direct band gap 1.89 eV (1.55 eV) for $1H - MoS_2$ using LDA + lo (GGA + lo) is in excellent agreements to recently calculated value 1.87 eV (1.58 eV) with LDA + PAW (GGA + PAW) based approach [30,31] and also finds very good agreements with other calculated values [33,36,48] as can be seen in Table 2. The calculated band gap of $1H - MoS_2$ within LDA is in good agreement with the band gap measured using complementary techniques of optical absorption, photoluminescence and photoconductivity (1.80 eV) [34] of monolayer thick MoS_2. However, it is worth mentioning here that optical band gap is always smaller than fundamental band gap due to large excitonic binding energy. Our calculated electronic direct band gaps for $1H - MoS_2$ is almost double the calculated indirect band gap of corresponding bulk $2H - MoS_2$. The band gap problem, however, can be addressed more accurately by using alternative methods such as GW approximation or using hybrid functionals which have not been carried out in this paper. In Table 2, we have also given the GW corrected band gap [31] for $1H - MoS_2$, which is approximately 0.7 eV higher than standard DFT + LDA band gap. Since reduced dimensionality can sometimes lead to magnetic behaviour in systems which are non-magnetic in bulk, we checked the possibility to have a spin-polarized magnetic ground state for $1H - MoS_2$, but it was found that two dimensional $MoS_2(1H - MoS_2)$ remains in a non-magnetic state.

Table 1
Calculated structural parameters of $2H - MoS_2$ and $1H - MoS_2$ using both LDA and GGA based localized orbitals method. The available results using PAW based approach have also been given for the purpose of comparison. Distance S–S is vertical distance between two sulphur atoms in S–Mo–S layer. Experimental values for $2H - MoS_2$ are also given.

Property	$1H - MoS_2$		$2H - MoS_2$		
	LDA	GGA	LDA	GGA	Exp.[a]
c/a ratio (in Å)	15 Å vacuum along c axis		3.84	4.01 4.35[c]	3.89
Lattice Constant (in Å)	3.13 3.11[b]	3.23 3.20[b]	3.13	3.23 3.18[c]	3.16
Bond Length(Mo–S) (in Å)	2.39 2.37[b]	2.45 2.42[b]	2.39	2.45 2.41[c]	2.41
Bond Angle(S–Mo–S) (in degree)	81.73 81.62[b]	80.88 80.69[b]	81.74	80.84	81.30
Distance(S–S) (in Å)	3.13 3.11[b]	3.18 3.13[b]	3.12	3.18	3.19

a = Ref. [7], b = Ref. [30,31], c = Ref. [38].

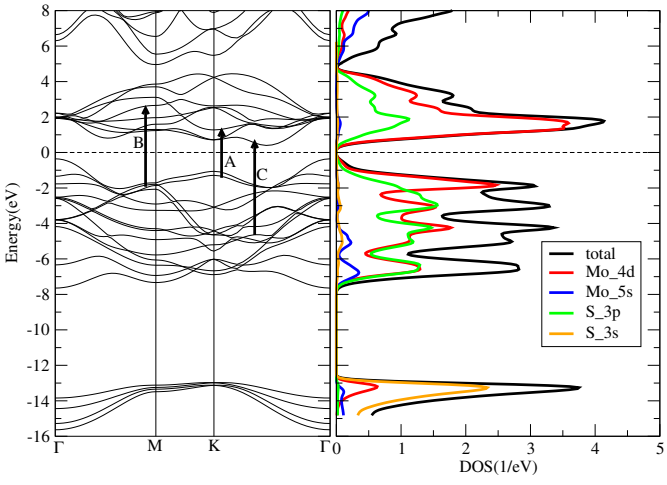

Fig. 2. Electronic band structure and corresponding total and partial density of states of $2H - MoS_2$ within LDA. All the partial DOS are multiplied by 3. Possible optical interband transitions are also shown in electronic band structure which are consistent with structure peaks in the imaginary part of dielectric function of $2H - MoS_2$.

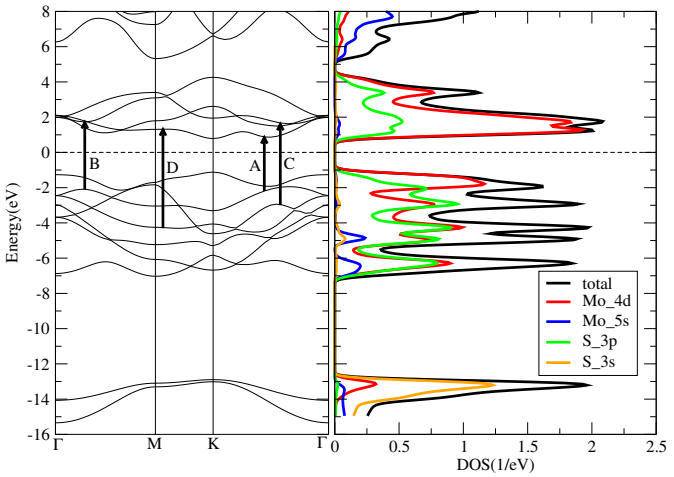

Fig. 3. Electronic band structure and corresponding total and partial density of states of $1H - MoS_2$ within LDA. All the partial DOS are multiplied by 1.5. Possible optical interband transitions are also shown in electronic band structure which are consistent with structure peaks in the imaginary part of dielectric function of $1H - MoS_2$.

3.3. Optical properties

Optical properties have been calculated in the energy range from 0 to 15 eV. Dielectric properties of compound having hexagonal symmetry can be calculated with electric vector E perpendicular or parallel to *c* axis. The complex dielectric functions $\varepsilon^{\perp}(\omega)$ and $\varepsilon^{\parallel}(\omega)$ are given by [8]

$$\varepsilon^{\perp}(\omega) = \frac{\varepsilon^{xx}(\omega) + \varepsilon^{yy}(\omega)}{2} \quad (1)$$

and

$$\varepsilon^{\parallel}(\omega) = \varepsilon^{zz}(\omega) \quad (2)$$

where $\varepsilon^{xx}(\omega)$, $\varepsilon^{yy}(\omega)$ and $\varepsilon^{zz}(\omega)$ are diagonal elements of the dielectric matrix $\varepsilon^{ij}(\omega)$. The imaginary part of dielectric function has been calculated from the band structure and real part from imaginary part using Kramers–Kronig relation:

$$\varepsilon_1(\omega) - 1 = \frac{2}{\pi} P \int_0^{\infty} \frac{\omega' \varepsilon_2(\omega')}{\omega'^2 - \omega^2} d\omega' \quad (3)$$

in which *P* denotes the principal value. Furthermore, optical properties calculations in SIESTA are based on the first order time dependent perturbation theory, but it uses self consistent ground state DFT energies and eigenfunctions which are pluged into the dipolar transition matrix elements. Energy loss function has been calculated from dielectric functions as

$$Im\left\{\frac{1}{\varepsilon(\omega)}\right\} = \frac{\varepsilon_2(\omega)}{\varepsilon_1^2(\omega) + \varepsilon_2^2(\omega)} \quad (4)$$

It has been found that LDA and GGA both gives similar optical properties, so all the graphs of optical properties reported in the paper have been obtained using LDA. Since only $E \perp c$ data is measured, experimental data of Beal and Hughes [12] is also plotted for E vector perpendicular to *c* axis for $2H - MoS_2$. Also, since there is no experimentally measured data available for single layer MoS_2 i.e. $1H - MoS_2$, so we have presented only the calculated optical properties for $1H - MoS_2$. Our calculated spectra shows good agreement with experimental data and required less than 0.7 eV shift to match with experimental data.

3.3.1. Interband transitions

Fig. 4 shows the calculated real and imaginary part of dielectric function for both E vector perpendicular and parallel to *c* axis for both $2H - MoS_2$ and $1H - MoS_2$. The dielectric functions are found highly anisotropic in low energy range (<7 eV) and become isotropic in high energy range. Our calculated data shows good agreement with the experimental data except for the excitonic peak at 1.9 eV for $2H - MoS_2$. However, it is emphasized that LDA/GGA is unable to yield any kind of excitonic effects but excitonic effects can be studied using more advanced method [39] such as solving Bethe–Salpeter equation. Imaginary part of dielectric functions ($\varepsilon_2^{\perp}(\omega)$ and $\varepsilon_2^{\parallel}(\omega)$) for $2H - MoS_2$ shows a structure with peaks at A, B and C as shown in Fig. 4 and corresponding energies are given in Table 3. Our calculated structure in $\varepsilon_2(\omega)$ finds very good agreements with earlier full potential calculations of Reshak and Auluck [8]. We have also identified the transitions in our calculated band structure (denoted as A, B, C in Fig. 2) that are responsible for these structures in $\varepsilon_2^{\perp}(\omega)$ and $\varepsilon_2^{\parallel}(\omega)$. Structure peak A is dominated by the interband transitions designated by A in electronic band structure in the vicinity of K high symmetry point as shown in Fig. 2. These transitions are mainly from the valence bands 1 and 2 below Fermi energy to the conduction bands 2 and 3 above the Fermi energy along MK and *K*Γ directions. Structure B is dominated by the interband transitions from the valence bands 1 and 2 below the Fermi energy to the conduction bands 4 and 5 above the Fermi energy in the vicinity of M high symmetry point and along KΓ direction. Structure C is mainly due to interband transitions from the valence bands 4 and 8 below the Fermi energy to the conduction bands 1 and 6 above the Fermi energy along ΓM and KΓ direction.

Imaginary part of dielectric functions($\varepsilon_2^{\perp}(\omega)$ and $\varepsilon_2^{\parallel}(\omega)$) for $1H - MoS_2$ shows structures at A(2.9 eV), B(3.8 eV), C(4.5 eV) and *D*(5.5 eV). It is found that additional structure peak at 3.8 eV appear for $1H - MoS_2$ in comparison with $2H - MoS_2$ but the location of other peaks are found at nearly same energy position for both $1H - MoS_2$ and $2H - MoS_2$. Structure A is dominated by the interband transitions(designated by A in electronic band structure in Fig. 3) from the valence bands 1, 2 below the Fermi energy to the conduction bands 1, 2 and 3 above the Fermi energy along ΓM and KΓ direction. Structure B is dominated by interband transitions from the valence bands 2 below the Fermi energy to the conduction bands 2 and 3 above the Fermi energy along ΓM direction and vicinity of M. Structure C is mainly due to interband transitions from the valence bands 3 below the Fermi energy to the conduction bands 2 and 3 above the Fermi energy along *K*Γ direction. Structure *D* is dominated by the interband transitions from the valence bands 4 below the Fermi energy to the conduction bands 1 above the

Table 2
Calculated electronic indirect band gap(in eV) between 'Γ' and 'K' points of $2H - MoS_2$ and direct band gap(in eV) of $1H - MoS_2$ at 'K' high symmetry point using LDA + localized orbitals and GGA + localized orbitals based method. Band gap using plane wave method, GW_0 corrected method and other theoretical methods along with experimental values are also given for the purpose of comparison.

Method	$2H - MoS_2$	$1H - MoS_2$
LDA + lo	0.75	1.89
GGA + lo	1.05	1.55
LDA+PAW[a]	0.72	1.87
GGA+PAW[a]	0.85	1.58
LDA + PAW+GW_0[a]	1.28	2.57
GGA + PAW+GW_0[a]	1.44	2.50
Other theory[b]	0.70, 1.06, 1.2	1.70, 1.78, 1.9
Exp.[c]	1.23	1.80

a = Ref. [30,31], *b* = Ref. [8,9,33,36,48], *c* = Ref. [34,49].

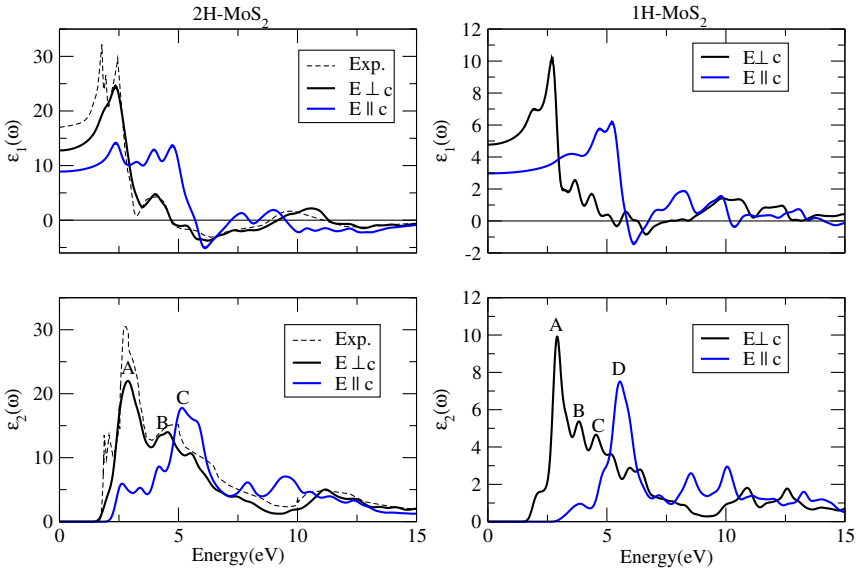

Fig. 4. Calculated frequency dependent real part ($\varepsilon_1^{\perp}$ and $\varepsilon_1^{\parallel}$) of dielectric function for electric vector E perpendicular and parallel to c axis for both $2H - MoS_2$ and $1H - MoS_2$. Experimental data (12) with dotted lines having E vector perpendicular to c axis is also plotted.

Table 3
Structure peak positions in imaginary part of dielectric function (ε_2), value of real part of dielectric function at zero energy($\varepsilon_1(0)$) and plasma energy for $2H - MoS_2$ and $1H - MoS_2$ are given. Numbers given in brackets are experimental values. Available theoretical data has also been given.

System	Peaks	$\varepsilon_1(0)$	Plasma Energy(eV)
$1H - MoS_2$	$A = 2.9$	$\varepsilon_1^{\perp}(0) = 4.8$	$E_p^{\perp} = 8.6, 15.7, 7.6^d, 15.6^d$
	$B = 3.8$	$\varepsilon_1^{\parallel}(0) = 3.0$	$E_p^{\parallel} = 16.0,16.8,18.6$
	$C = 4.5$		
	$D = 5.5$		
$2H - MoS_2$	$A = 2.9, 3.0^c$	$\varepsilon_1^{\perp}(0) = 12.8, 16.0^c$	$E_p^{\perp} = 9.2, 22.5, 8.5^d, 22.1^d$
	$B = 4.5, 4.5^c$	(16.8^a, 14.9^b)	(8.81^a,20.0^a,8.75^b,23.0^b)
	$C = 5.1, 5.5^c$	$\varepsilon_1^{\parallel}(0) = 8.9, 10.0^c$	$E_p^{\parallel} = 23.0$
		(9.0^b)	(23.0^b)

a = Ref. [12], b = Ref. [37], c = Ref. [8,9], d = Ref. [38].

Fermi energy in the vicinity of M. All the interband transitions mentioned above for both $2H - MoS_2$ and $1H - MoS_2$ are mainly due to transition from p valence bands of S to the d conduction bands of Mo.

It is worth mentioning that a particular structure peak in imaginary part of dielectric function (ϵ_2) may correspond to multiple interband transitions due to different bands number and different brillouin zone directions. Although, $2H - MoS_2$ and $1H - MoS_2$ have some of the structure peaks at same position (e.g. peaks at 2.9 eV and 4.5 eV) in ϵ_2, but their origin in electronic band structure is due to different brillouin zone directions and different band numbers (below and above the Fermi energy). On carefully observing the electronic band structure of both $2H - MoS_2$ and $1H - MoS_2$, we found that for $2H - MoS_2$ (in bulk phase) there are splitting of bands due to interlayer coupling in comparison with $1H - MoS_2$ (monolayer). Furthermore, it is well established that the effect of quantum confinement may change the positions and shape of the bands [48], which may result in different origin of interband transitions and the different direction of the transitions in brillouin zone despite same location of energy structure peak in bulk and monolayer MoS_2.

Calculated values of real part of dielectric function at zero frequency ($\varepsilon_1^{\perp}(0)$ and $\varepsilon_1^{\parallel}(0)$) for both $2H - MoS_2$ and $1H - MoS_2$ are

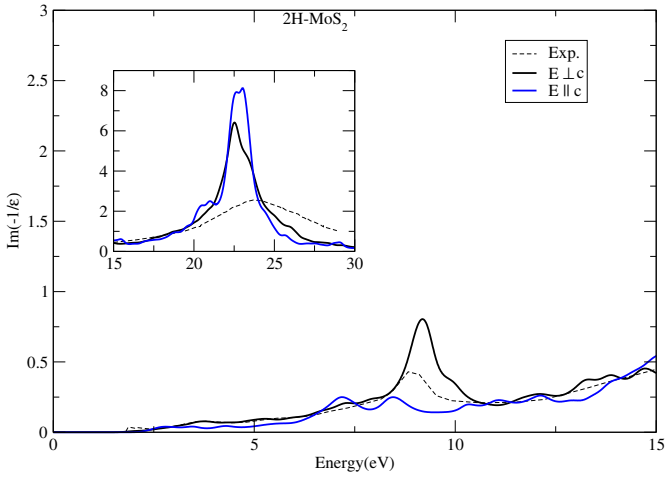

Fig. 5. Calculated energy loss function($Img(-1/\varepsilon)$) for electric vector E perpendicular and parallel to c axis for $2H - MoS_2$. Experimental data (12) with dotted line for E vector perpendicular to c axis is also plotted. Energy loss function in the range between 15 eV and 25 eV is also shown in the inset.

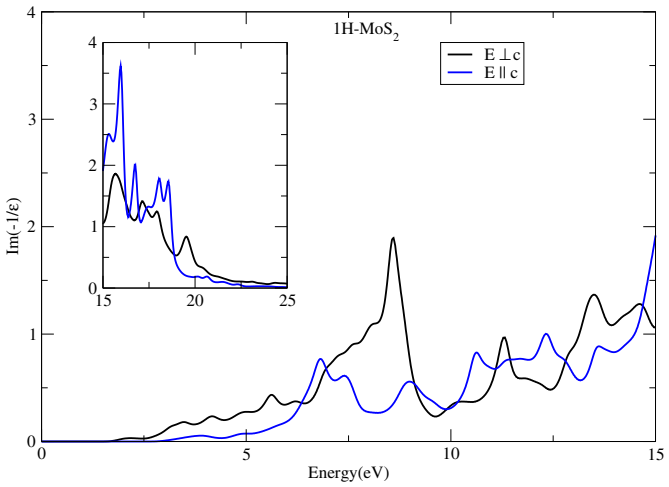

Fig. 6. Calculated energy loss function ($Img(-1/\varepsilon)$) for electric vector E perpendicular and parallel to c axis for $1H - MoS_2$. Energy loss function in the range between 15 eV and 25 eV is also shown in the inset.

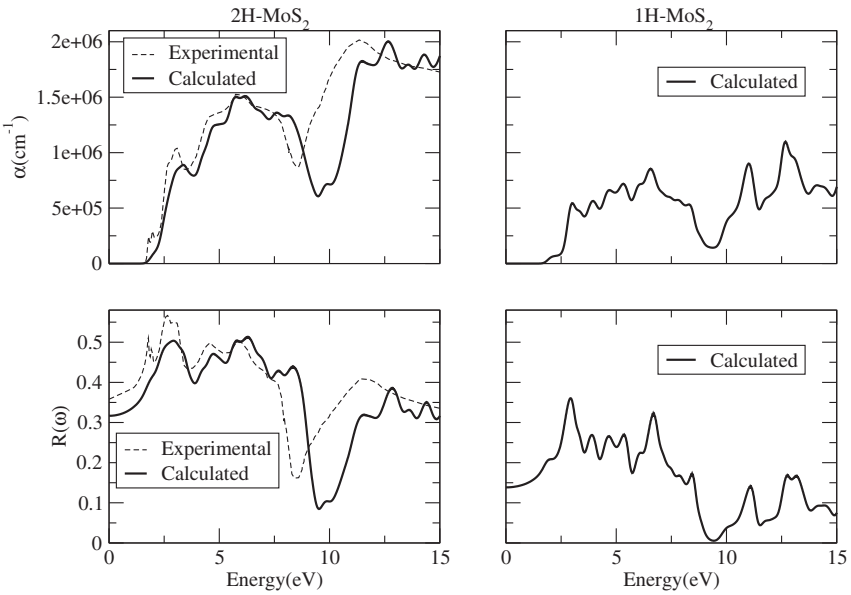

Fig 7. Calculated absorption coefficient (α) and reflectance (R) with electric vector E perpendicular to c axis for both $2H - MoS_2$ and $1H - MoS_2$. Experimental data (12) with dotted lines for $2H - MoS_2$ are also plotted for comparisons.

given in Table 3. However, $\varepsilon_1^{\perp}(0)$ for $2H - MoS_2$ is underestimated by 24% and 15% from two different experimental values [12,37], but $\varepsilon_1^{\parallel}(0)$ is very close to experimental value. Our calculated values also underestimate the full potential calculations [9] as shown in Table 3. The high positive value of ε_1 (0) is consistent with small band gap of $2H - MoS_2$. The calculated values of real part of dielectric function at zero frequency ($\varepsilon_1^{\perp}(0)$ and $\varepsilon_1^{\parallel}(0)$) for $1H - MoS_2$ are 4.8 and 3.0 respectively for E vector perpendicular and parallel to c axis. Very low positive value ε_1 (0) are consistent with the large band gap of $1H - MoS_2$.

3.3.2. Electron energy loss spectra

The electron energy loss spectra (EELS) for $2H - MoS_2$ in both perpendicular and parallel polarization along with experimental data for $E \perp c$ is shown in Fig. 5. Our calculated spectra shows a well defined sharp peak at 9.2 eV for E vector perpendicular to c axis which is consistent with energy loss peak at 8.81 eV of experimental spectra. This peak is associated with dips in $\varepsilon_2^{\perp}(\omega)$ at corresponding energy (see Fig. 4) and the point at which the $\varepsilon_1^{\perp}(\omega)$ curve crosses the zero axis from the negative side in this energy region. Also very prominent peak at 22.5 eV (shown as inset in energy loss spectra) consistent with experimental loss peak due to plasma resonance is also found. Our calculated energy loss spectra did not show any sharp well defined peak for E vector parallel to c axis in the region 0 eV–15 eV, but a prominent peak at 23.0 eV has been observed (shown as inset in energy loss spectra) which corresponds to the experimentally measured value of 23 eV. Our calculated plasmonic energies are also consistent with the values calculated with PAW based approach [38] as shown in Table 3.

Fig. 6 shows calculated electron energy loss spectra for both E vector perpendicular and parallel to c axis of $1H - MoS_2$. We find sharp energy loss peak at 8.6 eV for E vector perpendicular to c axis which is consistent with the loss peak in $2H - MoS_2$ and represents the collective plasmonic oscillations. A fairly sharp peak at 15.7 eV (shown in inset) for E vector perpendicular to c axis, which is not found in $2H - MoS_2$, but consistent with the loss peak 15.6 eV calculated with PAW based method [38] and is associated with the surface plasmons. A very sharp loss peak for E vector parallel to c axis is found at 16.0 eV (shown in inset) which can be attributed to the surface plasmons propagated along c axis. Also fairly sharp peaks are found at 16.8 eV and 18.6 eV (shown in inset) for E vector parallel to c axis, which are also most likely due to surface plasmons.

Fig 7 shows absorption and reflectance spectra of both $2H - MoS_2$ and $1H - MoS_2$ for E vector perpendicular to c axis. Experimental data of Beal and Hughes [12] are also plotted for $2H - MoS_2$. Strong minima in absorption and reflectance spectra is observed about 9 eV which is associated with the collective plasmons resonance. Also minima well in absorption and reflectance spectra of $1H - MoS_2$ is observed around 9 eV as compared to sharp minima in $2H - MoS_2$ and must be associated with the collective plasmons resonance in wide energy range of about 1 eV starting from 8.5 eV to 9.5 eV.

4. Conclusions

In summary, we studied the electronic and optical properties of layered MoS_2 using pseudopotential and localized atomic orbitals based SIESTA calculations. It is found that structural parameters of $2H - MoS_2$ and $1H - MoS_2$ are nearly identical. Electronic band structure and density of states calculations shows many similarities between $1H - MoS_2$ and $2H - MoS_2$ except the nature of the band gap which is found direct for $1H - MoS_2$ as compared to indirect for $2H - MoS_2$. It is found that states around Fermi energy are mainly due to the metal d states. From partial density of states we find a strong hybridization between metal d and chalcogen p states below the Fermi energy. LDA seems to be a good approximation for $1H - MoS_2$, while GGA gives the band gap close to the experimental value for $2H - MoS_2$. Optical spectra of $2H - MoS_2$ finds very good agreement with experimentally measured optical spectra. In the low energy region below 7 eV, dielectric functions are found to be anisotropic and becomes isotropic in high energy region. Additional structure revealing interband transition at 3.8 eV has been found for $1H - MoS_2$ as compared to $2H - MoS_2$. Interband transitions are found to be dominated by 3 p valence bands of S to the 4d conduction bands of Mo for both $1H - MoS_2$ and $2H - MoS_2$. Calculated electron energy loss spectra for $1H - MoS_2$ shows additional energy loss peaks for E vector parallel to c axis due to surface plasmons.

Acknowledgements

We gratefully acknowledge, SIESTA team for code. Ashok Kumar also acknowledges financial support from CSIR New Delhi in the form of Junior Research Fellowship.

References

[1] A.K. Geim, K.S. Novoselov, Nat. Mater. 6 (2007) 183.
[2] A.K. Geim, Science 324 (2009) 1530.
[3] C.N.R. Rao, A.K. Sood, K.S. Subrahmanyam, A. Govindraj, Angew. Chem. Int. Ed. 48 (2009) 7752.
[4] J.O. Sofo, A.S. Chaudhari, G.D. Barber, Phy. Rev. B 75 (2007) 153401.
[5] C.H. Jin, F. Lin, K. Suenaga, S. Iijima, Phy. Rev. Lett. 102 (2009) 195505.
[6] O.V. Sedelnikova, L.G. Bulusheva, A.V. Okotrub, J. Chem. Phys. 134 (2011) 244707.
[7] J. Wilson, A. Yoffe, Adv. Phys. 18 (1969) 193.
[8] A.H. Reshak, S. Auluck, Phy. Rev. B 68 (2003) 125101.
[9] A.H. Reshak, S. Auluck, Phy. Rev. B 71 (2005) 155114.
[10] A.R. Beal, J.C. Knights, W.Y. Liang, J. Phys. C.: Sol. Stat. Phys. 5 (1972) 3540.
[11] H.P. Hughes, W.Y. Liang, J. Phys. C.: Sol. Stat. Phys. 7 (1974) 1023.
[12] A.R. Beal, H.P. Hughes, J. Phys. C.: Sol. Stat. Phys. 12 (1979) 881.
[13] L. Rapoport, Y. Bilik, Y. Feldman, M. Homyonfer, S. Cohen, R. Tenne, Nature 387 (1997) 791.
[14] C. Lee, Q. Li, W. Kalb, X.Z. Liu, H. Berger, R.W. Karpic, J. Hone, Science 328 (2010) 76.
[15] B. Hinnemann, P. Moses, J. Bonde, K. Jorgensen, J. Nielsen, S. Horch, I. Chorkendorff, J. Norskov, J. Am. Chem. Soc. 127 (2005) 5308.
[16] T.F. Jaramillo, K.P. Jorgensen, J. Bonde, J.H. Nielsen, S. Horch, I. Chorkendorff, Science 317 (2007) 100.
[17] T. Todorava, R. Prins, T. Weber, J. Catal. 246 (2007) 109.
[18] M. Sun, A. Nelson, J. Adjaye, J. Catal. 226 (2004) 32.
[19] P. Raybaud, J. Hafner, G. Kresse, S. Kasztelan, H. Toulhoat, J. Catal. 189 (2005) 129.
[20] P.G. Moses, B. Hinnemann, H. Topsoe, J.K. Norskov, J. Catal. 248 (2007) 188.
[21] J.V. Lauritsen, J. Kibsgaard, G.H. Olesen, P.G. Moses, B. Hinnemann, S. Helveg, J.K. Norskov, B.S. Clausen, H. Topsoe, E. Laegsgaard, F. Besenbacher, J. Catal. 249 (2007) 220.
[22] J. Lauritsen, J. Bollinger, E. Laegsgaard, K. Jacobsen, J.K. Norskov, B. Clausen, H. Topsoe, F. Besenbacher, J. Catal. 221 (2004) 510.
[23] J. Lauritsen, S. Helveg, E. Laegsgaard, I. Stensgaard, B. Clausen, H. Topsoe, E. Besenbacher, J. Catal. 197 (2001) 1.
[24] G. Kline, K. Kam, R. Ziegler, B. Parkinson, Solar Energy Mater. 6 (1982) 337.
[25] J. Wilcoxon, T. Thurston, J. Martin, J. Nanostructured Mater. 12 (1999) 993.
[26] K. Novoselov, D. Jiang, F. Schedin, T. Booth, V. Khotkevich, S. Morozov, A. Geim, Proc. Natl. Acad. Sci. U.S.A. 102 (2005) 10451.
[27] S. Helveg, J. Lauritsen, E. Laegsgaard, I. Stensgaard, J. Norskov, B. Clausen, H. Topsoe, F. Besenbacher, Phy. Rev. Lett. 84 (2000) 951.
[28] J.N. Coleman, M. Lotya, A. O'Neill, Science 331 (2011) 568.
[29] B. Radisavljevic, A. Radenovic, J. Brivio, V. Giacometti, A. Kis, Nat. Nanotechnology 6 (2011) 147.
[30] C. Ataca, H. Sahin, E. Akturk, S. Ciraci, J. Phy. Chem. C 115 (2011) 3934.
[31] C. Ataca, S. Ciraci, J. Phys. Chem. 115 (2011) 13303.
[32] J. He, K. Wu, R. Sa, Q. Li, Y. Wei1, App. Phys. Lett. 96 (2010) 082504.
[33] H.S.S. Ramkrishana Matte, A. Gomathi, A.K. Manna, D.J. Late, R. Dutta, S.K. Pati, C.N.R. Rao, Angew. Chem. Int. Ed. 49 (2010) 4059.
[34] K.F. Mak, C. Lee, J. Hone, J. Shan, T.F. Heinz, Phy. Rev. Lett. 105 (2010) 136805.
[35] A. Enyashin, S. Gemming, G. Seifert, Eur. Phys. J. 149 (2007) 103.
[36] S. Lebegue, O. Eriksso, Phy. Rev. B 79 (2009) 115409.
[37] K. Zeppenfeld, Opt. Commun. 1 (1970) 377.
[38] P. Johari, V.B. Shenoy, ACS Nano 5 (2011) 5903.
[39] T. Olsen, K. W. Jacobsen, K. S. Thygesen, http://arxiv.org/abs/1107.0600.
[40] J.M. Soler, E. Artacho, J.D. Gale, A. Garc1ia, J. Junquera, P. Ordejon, D.S. Portal, J. Phys.:Condens. Matter 14 (2002) 2745.
[41] P. Ordejon, E. Artacho, J.M. Soler, Phys. Rev. B 53 (1996) 10441.
[42] D. Sanchez-Portal, P. Ordejon, E. Artacho, J.M. Soler, Int. J. Quantum Chem. 65 (1997) 453.
[43] E. Artacho, D. Sanchez-Portal, P. Ordejon, A. Garcia, J.M. Soler, Phys. Stat. Sol. 215 (1999) 809.
[44] N. Troullier, J.L. Martins, Phy. Rev. B 43 (1991) 1993.
[45] N. Troullier, J.L. Martins, Phy. Rev. B 43 (1991) 8861.
[46] G.P. Kerker, J. Phys. C.: Solid St. Phys. 13 (1980) L189.
[47] D.R. Hamann, M. Schluter, C. Chiang, Phys. Rev. Lett. 43 (1979) 1494.
[48] A. Kuc, N. Zibouche, T. Heine, Phys. Rev. B 83 (2011) 245213.
[49] K. Kam, B. Parkinson, J. Phy. Chem. 86 (1982) 463.